The Potential for Grain Refinement of Wire-Arc Additive Manufactured (WAAM) Ti-6Al-4V by ZrN and TiN Inoculation

J.R. Kennedy, A.E Davis, A.E. Caballero, S. Williams, E.J. Pickering, P.B. Prangnell

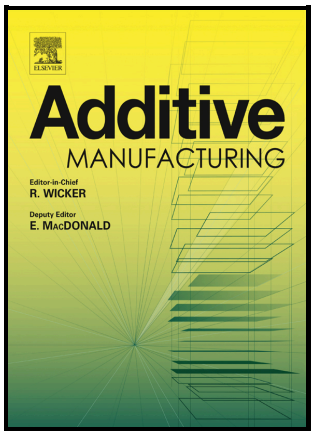

PII: S2214-8604(21)00093-2

DOI: https://doi.org/10.1016/j.addma.2021.101928

Reference: ADDMA101928

To appear in: *Additive Manufacturing*

Received date: 24 November 2020
Revised date: 15 January 2021
Accepted date: 21 February 2021

Please cite this article as: J.R. Kennedy, A.E Davis, A.E. Caballero, S. Williams, E.J. Pickering and P.B. Prangnell, The Potential for Grain Refinement of Wire-Arc Additive Manufactured (WAAM) Ti-6Al-4V by ZrN and TiN Inoculation, *Additive Manufacturing,* (2020) doi:https://doi.org/10.1016/j.addma.2021.101928

Additive Manufacturing, Volume 40, April 2021 Artcle number 101928
DOI: 10.1016/j.addma.2021.101928

The Potential for Grain Refinement of Wire-Arc Additive Manufactured (WAAM) Ti-6Al-4V by ZrN and TiN Inoculation

*J. R. Kennedy[1], A.E Davis[1], A.E. Caballero[2], S. Williams[2], E.J. Pickering[1], P.B. Prangnell[1]

[1]University of Manchester, Department of Materials
Manchester, United Kingdom, M13 9PL

[2]Welding Engineering and Laser Processing Centre, Cranfield University
Bedfordshire, United Kingdom, MK43 0PL

(*Corresponding author: jacob.kennedy@manchester.ac.uk)

ABSTRACT

Wire-Arc Additive Manufacturing (WAAM) of large near-net-shape titanium components has the potential to reduce costs and lead-time in many industrial sectors including aerospace. However, with titanium alloys, such as Ti-6Al-4V, standard WAAM processing conditions result in solidification microstructures comprising large cm-scale, <001> fibre textured, columnar β grains, which are detrimental to mechanical performance. In order to reduce the size of the solidified β-grains, as well as refine their columnar morphology and randomise their texture, two cubic nitride phases, TiN and ZrN were investigated as potential grain refining inoculants. To avoid the cost of manufacturing new wire, experimental trials were performed using powder adhered to the surface of the deposited tracks. With TiN particle additions, the β grain size was successfully reduced and modified from columnar to equiaxed grains, with an average size of 300 µm, while ZrN powder was shown to be ineffective at low addition levels studied. Clusters of TiN particles were found to be responsible for nucleating multiple β Ti grains. By utilizing the Burgers orientation relationship, EBSD investigation showed that a Kurdjumov-Sachs orientation relationship could be demonstrated between the refined primary β grains and TiN particles.

KEYWORDS

Additive manufacturing, Grain refinement, Inoculation, Titanium, Ti64, WAAM

1.0 Introduction

Titanium (Ti) alloys are one of the most commonly used aerospace materials [1], owing to their high specific strength, good corrosion and oxidation resistance[2]. Additive manufacturing (AM) is a particularly attractive path to reducing the high cost [3] of conventional wrought Ti parts, which are frequently associated with high buy-to-fly ratios [4]. There are a variety of AM technologies [5] which have been applied to Ti-6Al-4V (Ti64), the most common Ti alloy used in aerospace, [6–8]. High deposition rate wire-fed methods, like Wire-Arc Additive Manufacturing (WAAM), are particularly suited for the production of airframe parts because of their ability to efficiently produce larger-scale components which are meters in length [9]. However, in AM processes with Ti64 there is a propensity to form large <001> textured β grains during solidification, which affects the α transformation texture and leads to mechanical anisotropy.

In the WAAM process a wire is fed into a melt pool, created by a plasma-transferred arc. Sequential layers produced by single, or multiple, melt tracks are deposited on top of one another to build up a component [10]. In most Ti alloys, without substantial modification of the deposition conditions [11–14], this results in solidification occurring by epitaxial growth from the fusion boundary with the re-melted neighbouring tracks, where the β grains re-form on

heating above the transus temperature in each deposition cycle. This results in solidification structures consisting of large columnar β grains with a common <100> direction aligned closely to the build direction [9,15]. This <100> fibre-textured parent grain structure, strongly influences the room temperature α-β transformation microstructure, which can cause mechanical anisotropy in components [9,15]. The propensity to form coarse columnar β grains during multi-pass melt pool solidification is particularly strong in the case of Ti64 because there is minimal solute partitioning in this alloy [11]. When combined with the steep thermal gradients found at the solidification front in a translated-heated melt pool [16], this results in little constitutional undercooling, which prevents nucleation ahead of the growth front. Subsequent solid-state phase transformation to the α phase does not fully eliminate the memory of this solidification structure on the mechanical properties. This is partly because there is a Burgers Orientation relationship (BOR) between the α variants that nucleate on cooling and their parent β grains, but also because α colonies nucleate on the prior β grain boundaries which causes plastic heterogeneity, particularly in transverse loading [17].

In order to improve the negative effects of a coarse β grain structure formed during solidification on their mechanical properties and eliminate mechanical anisotropy, to date two main approaches have been utilized to refine this in WAAM; inter-pass deformation and alloy modification. Inter-pass deformation can be implemented by using techniques such as rolling [18], or peening [19], to deform the surface of the deposit before the next layer/melt track is applied. In this approach the stored energy from the inter-pass deformation, combined with the heat input from subsequent deposition passes, results in β recrystallization during reheating through the β transus [20]. This method is attractive as there is no change in the alloy composition; however, it adds an additional processing step which slows production time. Alloy modification approaches include; i) grain refinement by solute additions and ii) inoculation. Both approaches are frequently used in unison in efficient grain refining systems in other metals (e.g. TiB_2 in Al alloys [21]). Growth restriction can be rationalised in terms of the diffusivity of the solute in the liquid and the degree of partitioning at the solidification front [22]. However, nucleation is still limited by the heterogeneous sites available in the liquid [23]. In Ti alloys solutal growth restriction by elements, such as boron [24] or silicon [25], has been shown to be effective in reducing the width of columnar grains, but less effective in inducing a columnar to equiaxed transition (CET), [26]. Unfortunately, such alloy additions frequently have unwanted side effects, such as the formation of brittle second phases (e.g. TiB_2 [27]). Inoculation is a method of grain refinement based on introducing efficient nucleants into a melt by the addition of artificial particles, or via high temperature precipitation reactions before the primary phase forms [28]. Inoculants are selected to minimize the energy barrier for nucleation, which requires a low interfacial energy between the inoculant particle and the primary solidifying phase [29]. There are currently no accepted commercial systems for inoculation of cast Ti alloys, due to their high reactivity, greater melting temperature and the detrimental effects of introducing brittle phases into such high strength materials [21]. More recently, the novel technique of isomorphic inoculation, has been proposed to circumvent these issues [30]. However, its implementation is difficult in practice as careful control of superheat and melt contact time is required to avoid dissolution of the particles.

Previous studies on grain refinement with Ti in AM have mainly focused on solutal growth restrictors and La_2O_3 inoculants [13,25,31]. As noted above, solutal growth restrictors do not on their own necessarily result in the formation of an equiaxed grain structure, but have been demonstrated to reduce the size of the coarse columnar grains [32]. La_2O_3 has been shown to

be an effective innoculant for Ti alloys, but in order to be effective requires the addition of solute growth restricting elements, such as B [31], or significant levels of conventional Ti alloying elements for example, Cr and Mo, which are not present in Ti64 [13]. It is therefore desirable to find inoculant additions which can be effective during AM of Ti64 without other solute additions and at a lower cost.

The cubic nitride phases, ZrN and TiN have recently been shown by Qiu et al. [33], to be effective Ti grain refiners in casting experiments with a model β stabilized Ti-13Mo alloy. In this work a refinement effect was found at relatively low addition levels of above ~ 0.5 wt.% by direct TiN addition, or by using ZrN. In the case of the ZrN additions, it was claimed that the ZrN first dissolved in the melt and TiN was then precipitated, which acted as nucleation sites. Although in pure Ti, theoretically, this requires nitrogen contents in excess of 5 wt% [34], grain refinement was seen at lower addition levels of 0.4 wt% and it was suggested that the presence of Zr and Mo allowed TiN to form at lower concentrations, with grain refinement also assisted by solutal growth restriction. It was further demonstrated in this work that the cubic (NaCl prototype) -TiN phase could form either BCC//FCC Kurdjumov-Sachs or Nishiyama-Wasserman orientation relationships (ORs) with the matrix and therefore that TiN is an effective nucleant for β-Ti. However, there are few other publications that report on the effectiveness of cubic nitride inoculants in Ti alloys and none on their application to AM processes.

Here we have, therefore, investigated the potential for cubic nitrides to act as efficient grain refiners during the WAAM process. TiN and ZrN particles were added to Ti64 builds to test their ability to refine the, normally obtained, undesirable coarse grain size and strong texture of the primary β phase. The stabilities of the nitride phases were also evaluated thermodynamically in order to assess their particle-melt pool survivability. To confirm the particles nucleation efficiency, the ORs between the nitrides and β matrix grains were investigated in detail by EBSD, by taking into account the BOR with the α phase present in the matrix at room temperature.

3.2 Experimental Procedure

To test the ability of TiN to refine the β solidification microstructure of Ti64 during WAAM, a simple experimental method was employed, whereby TiN and ZrN powders were premixed with a polyurethane adhesive before being applied as a thin coating to the top of each deposited layer, after which a new layer was added using a standard WAAM setup. The minimum amount of adhesive (polyurethane) was used to prevent the powder being blown off the deposit by the plasma arc pressure (a similar method for testing inoculants has been employed previously by Bermingham et al. [31]). The TiN powder was purchased from Sigma-Aldrich and had a maximum particle size of 3 μm, while ZrN was purchased from Fisher Scientific as 325 mesh particles, i.e. with a maximum size of 44 μm, the larger size was chosen due to availability. The purity of the ZrN was reported as 99.5% pure, while the TiN was reported to be 75-80 wt%, (47-54 at%) Ti with a balance of N.

Standard geometry linear WAAM wall test samples were deposited one track wide and 20 layers high, on a Ti64 rolled plate substrate, inside a low oxygen (600ppm) enclosure. Four walls were produced using identical build parameters, but with different additions made to the last 10 layers; i.e., in all samples the first 10 layers were deposited as purely Ti64, to first reach a representative steady state, before applying any inoculant particles. The four samples produced are identified as: i) 'Ti64', manufactured with just Ti64 alloy wire, as a control reference; ii) 'Ti64-P', built using polyurethane adhesive, but without any inoculant powder; iii) 'Ti64-TiN', using polyurethane adhesive with TiN powder; and iv) 'Ti64-ZrN', using polyurethane adhesive with ZrN powder. This sample set thus allowed the effects of the polyurethane bonding agent

and TiN and ZrN powders to be deconvoluted and compared to the baseline standard. The WAAM deposition parameters are provided in Table 1 and a schematic of the sample build methodology is shown in Figure 1. After deposition, the walls were removed from their substrates and ND-TD cross sections were metallographically prepared, with a final polishing step of 0.25 µm colloidal silica, for SEM analysis, and etched with krolls reagent for optical imaging. Bulk α - phase EBSD orientation maps were obtained using a FEI Sirion FEG-SEM equipped with an Oxford Instruments' (OI) Nordlys Nano EBSD detector, operated at 20 kV, and indexed with OI AZtec and analysed with Channel 5 software. Further higher-resolution analysis was carried out using a Zeiss Sigma or FEI Magellan FEG-SEMs, with OI Nordlys Nano EBSD and Xmax^{n} SDD-EDX detectors.

Table 1: WAAM deposition parameters

WAAM build parameters	
Travel Speed	5 (mm s^{-1})
Current	160 (A)
Wire Diameter	1.2 (mm)
Layer Height	~1.1 (mm)
Plasma Gas Flow	0.013 (L s^{-1})
Wire Feed Speed	2 (m min^{-1})

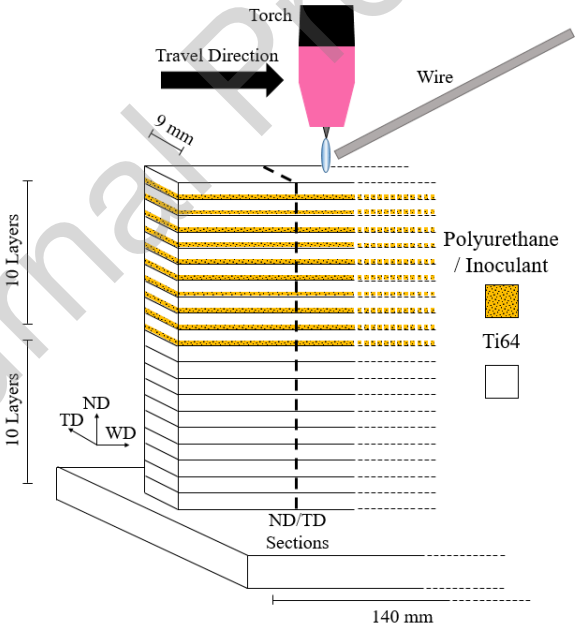

Figure 1: Test sample schematic and reference frame. The location of cross sections taken for metallographic investigation are indicated.

In the WAAM process solid-state transformation from β to α after solidification occurs with a high cooling rate and the small fraction of fine retained β makes evaluation of the β solidification microstructure difficult by direct observation. However, the BOR ($\{110\}_\beta // \{0001\}_\alpha$ and $\langle 111\rangle_\beta // \langle 11\bar{2}0\rangle_\alpha$) between the parent β and transformed α still makes it possible to interpret any prior orientation relationship that existed between the solidified β grains and inoculating particle. Algorithms are also available that can reconstruct the parent β phase grain

orientations from the orientations of the resultant α phase variants measured at room temperature using electron back scatter diffraction (EBSD) [35]. Here, the methodology of Davies and Wynne [36,37] was implemented to reconstruct the parent β phase from α EBSD maps.

4.0 Results

4.1 Compositions of the Deposited Materials

Bulk chemical analysis was carried out by inductively coupled plasma (ICP) and gas emission infra-red absorption fusion (LECO) tests on each test piece, in order to confirm the concentrations of inoculant particles and the amount of C that had entered the melt pool from the polyurethane (shown in Table 2). From this analysis the addition levels of C, TiN and ZrN were determined (Table 3). As expected, when the polyurethane adhesive was used the C content increased slightly in each case, with more C being added with the TiN powder than with the other samples which were nearly identical. From this analysis it can be seen that addition levels of 0.26 wt% TiN and 0.45 wt% ZrN were achieved in the as-built samples with only low levels of associated carbon (<0.08 wt%). It should be noted that these levels represent the total level of particle additions which entered the deposit, during interaction with the melt there will be some dissolution of particles changing the distribution and addition level present when solidification occurs.

Table 2: Bulk compositions (wt%) measured for the top 10 layers of each build.

wt%	Ti	Al	V	Fe	O	N	C	Zr
Ti64	89.43	6.22	3.95	0.20	0.17	0.01	0.02	0
Ti64-P	89.51	6.13	3.95	0.19	0.16	0.01	0.05	0
Ti64-TiN	89.58	6.10	3.78	0.22	0.19	0.07	0.08	0
Ti64-ZrN	89.19	6.11	3.86	0.18	0.16	0.065	0.05	0.39

Table 3: Calculated addition levels from bulk compositions

wt% additions	C	TiN	ZrN
Ti64	0	0	0
Ti64-P	0.03	0	0
Ti64-TiN	0.06	0.26	0
Ti64-ZrN	0.03	0	0.45

4.2 Baseline samples

EBSD β-phase reconstructed maps showing cross-sections of roughly the top 10 layers (ND-TD plane) from the baseline Ti64 and adhesive only as-built samples (Ti64 and Ti64-P respectively) are compared in Figure 2. The standard Ti64 sample is shown in Figure 2a and has a typical WAAM grain structure [8,15,38], comprising large mm-scale columnar primary β grains. In the EBSD maps, the grains tilt outwards towards the wall surfaces, following the melt pool surface, which for a single track wide wall is convex with respect to ND in the ND-TD plane (similar to the bead profile) [39]. From comparison with Figure 2b, it can be observed that when the adhesive was added a similar grain structure was obtained with no appreciable change in grain size; i.e., there was no obvious evidence of the low levels of carbon contamination from the adhesive influencing the results. The near top surface region of both walls can be seen to exhibit a thin layer of smaller β grains with different orientations. These grains probably formed by nucleation from the liquid bead surface as a result of the chill effect from the Ar shielding gas. However, they are only seen in the last pass as they are re-melted by the heat source when the next layer is added, resulting in deposits dominated by columnar grains that formed by

continuous growth from the fusion boundary for each melt track. Within the columnar grains weak orientation gradients are also noticeable, of ~ 2-5° (as seen by the change in colours in the orientation maps), indicating that there can be small changes in the crystal orientations during solidification. However, this does not break up the columnar structure.

As expected [8,15,38], in the both baseline samples produced without the addition of nitride inoculants, the β columnar grains were highly textured with a common <100> growth direction oriented near to the build direction (ND) (Figure 2 c & d). In Figure 2 the few grains present have grown up through multiple layers, as solidification occurred epitaxially from the fusion boundary during each pass without any new nucleation, after the β phase in the deposited layers reformed on re-heating above the β transus as the torch approached. This texture thus develops by growth selection of orientations with an <001> preferential growth direction closest to normal to the melt pool surface. The red colouration in the IPF map also indicates strong <001> grain alignment near to ND for both samples (Figure 2a). In the accompanying pole figures in Figure 2c it can be seen that in these samples, rotation around ND is quite limited and the texture is dominated by a single near-cube orientation (i.e., near to {001}//ND, <010>//WD) with a limited spread around the <001>//ND fibre. The stronger yellow hue in the IPF//ND map for the Ti64-P sample (Figure 2b) is caused by a greater tilt of the <001> grain alignment towards WD (Figure 2d). However, the grain size is very similar in both samples and, because of the low number of grains analysed, more data from multiple sections would be required to determine if there is a statistically reproducible difference between the two samples.

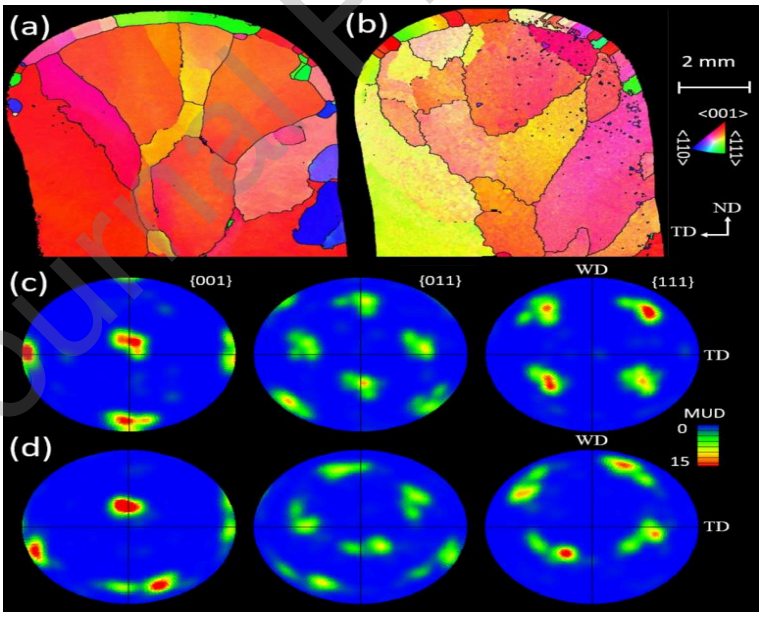

Figure 2: IPF//ND reconstructed β orientation EBSD maps for the baseline WAAM samples built; (a) without any additions (Ti64) and (b) with polyurethane adhesive added between layers (Ti64-P); their respective pole figures are shown in (c) and (d).

4.3 TiN additions

In order to evaluate the potential for utilising TiN as a Ti64 grain refiner in the WAAM process, a β reconstructed EBSD orientation map was produced from the entire ND-TD cross

section of the Ti64-TiN build, up from the substrate, and is shown in Figure 3. An optical image and measured α IPF//ND orientation map are also presented as the change in solidification structure is also evident in the transformed structure. The bottom of this build, which was deposited without nitride addition, has the expected columnar microstructure dominated by large columnar β grains. The texture from this region, depicted in Figure 3e, matches closely with that obtained from the top 10 layers of the baseline Ti64 wall in Figure 2c. This again shows a strong dominant cube orientation with preferential <001> alignment close to ND, and a slight tilt towards WD, but a smaller spread around ND relative to that seen in Figure 2c. However, the top ten layers produced with the TiN powder addition had a markedly different grain structure to the bottom wall section, or when the polyurethane adhesive was applied without any inoculant (Figure 2b).

It can be seen in Figure 3c, that with the addition of TiN powder the grain size has been dramatically reduced from near cm-scale large columnar grains to an average diameter of ~300 µm, with a much more equiaxed morphology (determined from the equivalent circular diameter of grains delineated by 15° misorientation boundaries in the reconstructed β EBSD). A very distinct demarcation can also be observed between the layers deposited, with (top) and without (bottom) TiN additions, with the growth of the columnar grains being abruptly halted when TiN powder was applied. In addition to changing the morphology to equiaxed and greatly refining the size of the β grains, the strong <001> texture seen in Figure 2 was replaced by a near random distribution of orientations in the top section of the sample; as shown in Figure 3d, where no specific orientations are now strongly favoured. This is exemplified by the low intensity maxima seen in the pole figures which are less than twice random in the refined region, compared to eighteen times random in the lower part of the wall that was built without inoculation (Figure 3e).

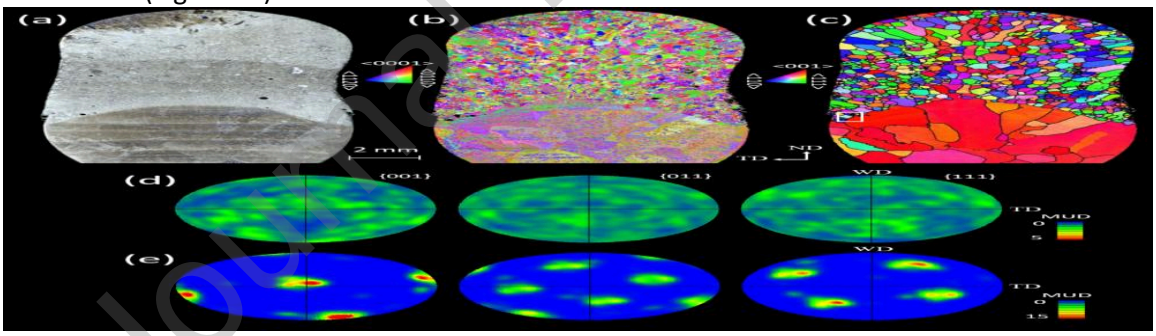

Figure 3: ND/TD cross section of sample produced with TiN additions (a) optical image (b) measured α IPF//ND orientation map (c) reconstructed IPF//ND β orientation map, (d) and (e) the corresponding β texture obtained from the top TiN doped layers and the base of the wall before the TiN powder was applied, respectively.

From comparison of Figure 2 and Figure 3 it is evident that the TiN powder added to each layer was highly effective as a grain refiner, in that both the grain size and texture strength were greatly reduced. In refined cast products, inoculating particles that have actively nucleated a new grain are normally found close to their centre and a reproducible orientation relationship can be measured between the inoculant particle and the solidified primary phase matrix [33]. With the WAAM materials careful investigation by serial sectioning of the sample produced with TiN additions, combined with SEM-BSE imaging, did not reveal any grains with this idealised single particle 'inoculant-centric' behaviour. Rather, the inoculants were found to be

concentrated in clusters of varying size with multiple β grains radiating from them, as shown in Figure 4c. Each cluster was made up of as many as ~ 100 small TiN particles with individual orientations (Figure 4d). Examples of Ti infiltration into the clusters can be seen in the high-resolution image inset in Figure 4b. The distribution of these clusters can be seen as unetched regions in the optical images presented in Figure 3a and Figure 4a. The clusters are well distributed throughout the layers where they were added, qualitatively, the distribution appears leaner in the centre of the build with a bias towards the edges. From this study it is not obvious if this is due to fluid flow within the molten pool or the adhesive addition method. Furthermore the clusters are found throughout the depth of the layers, the clusters shown in Figure 4 being located at the root of the first pass containing TiN, and no obvious layering is evident in their distribution shown in the presented maps. When viewed by imaging and EBSD-β reconstruction in the SEM (Figure 4), the relationship between the primary β grain structure and the specific particles that had acted as inoculants was therefore difficult to interpret. A statistical method was therefore used to identify the prevalent crystallographic orientation relationship between the nucleating particles and the matrix, which will be discussed further below.

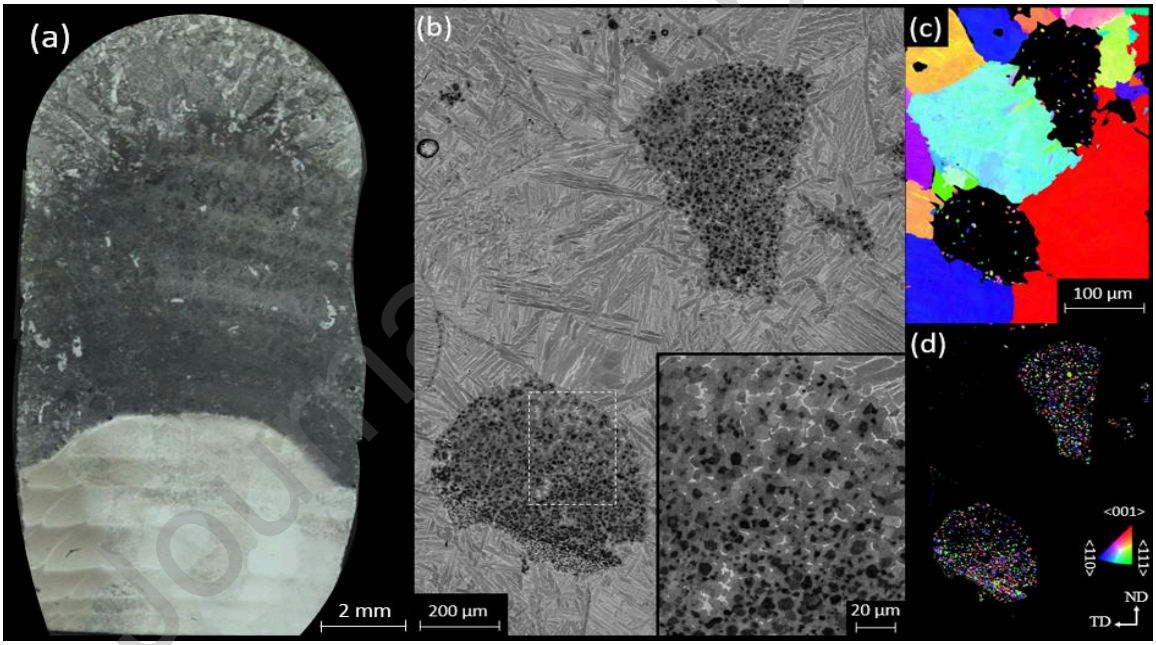

Figure 4: Examples of TiN particle clusters found in the Ti64-TiN WAMM build from region indicated in Figure 3c ; (a) etched optical image (TiN clusters remain unetched) (b) imaged by BSE, (c) IPF//ND colour contrast EBSD map of the reconstructed matrix β grain structure, and (d) the TiN particle orientations within each cluster indexed by EBSD.

4.4 ZrN additions

Figure 5 shows a comparable ND/TD reconstructed β EBSD map from the Ti64-ZrN build, to that for the Ti64-TiN sample provided in Figure 3. Similar to the base line samples, the cross sections exhibited microstructures composed mainly of large columnar grains oriented with a preferential <001> growth direction close to ND, with a slight tilt towards WD. Unlike for the Ti64-TiN build, no significant grain refinement was observed. When compared to the Ti64, or

the Ti64-P builds, the texture exhibited a slightly greater spread of orientations by rotation about the common <001>//ND axis, and there was more evidence of near-surface nucleated grains. However, given the few grains present in each sample it was unclear if this was a statistically significant difference. Furthermore, as can be seen in Figure 5b and c, a similar orientation spread was present in the top and bottom of the wall, and this behaviour could thus not be attributed to the ZrN additions.

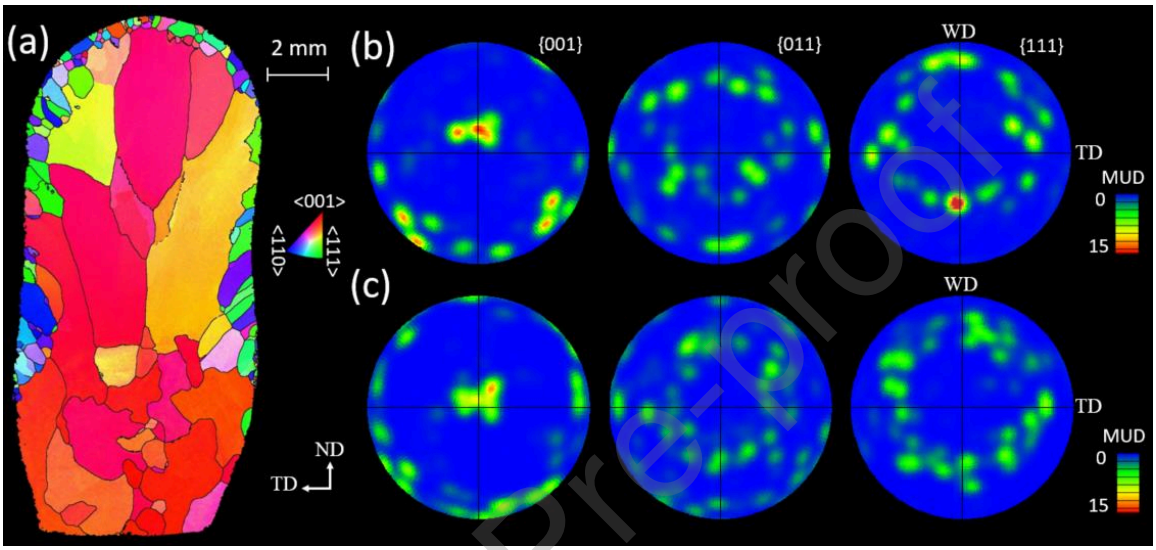

Figure 5: Reconstructed β phase EBSD orientation data from the Ti64 WAAM sample produced with ZrN additions; (a) an IPF//ND β orientation map of the whole wall section, (b) and (c) the corresponding textures from the top ZrN doped layers and the base of the wall, before ZrN powder was applied, respectively.

In the Ti64-ZrN samples the locations of regions that contained remnants of ZrN particles were identifiable in SEM BSE images from the presence of bright contrast regions associated with a higher local Zr concentration, as shown in Figure 6. These regions can be seen to be Zr rich in the EDS map in Figure 6. The Zr rich bands were frequently located near but not on β grain boundaries (Figure 6a), and there was no suggestion that they had acted as grain nucleation sites. A few Zr rich solute bands were also found in which surviving particles could be identified, such as the polycrystalline particle shown in Figure 6c that was located near to the sample's surface (wall face). This single polycrystalline particle can be seen to have an irregular shape and was identified by its high Zr content. The EDS maps in Figure 6 provide examples of surviving ZrN particles that are in various stages of dissolving, while circulating in the melt pool, which has left behind 'frozen in' Zr solute-rich liquid. These solute-rich trails are formed where Zr was released locally into the melt as the particles dissolved and has subsequently been partially dispersed by diffusion and liquid shear, caused by convective flow [40]. However, during solidification the Zr may also have become more concentrated locally due to solute partitioning during freezing.

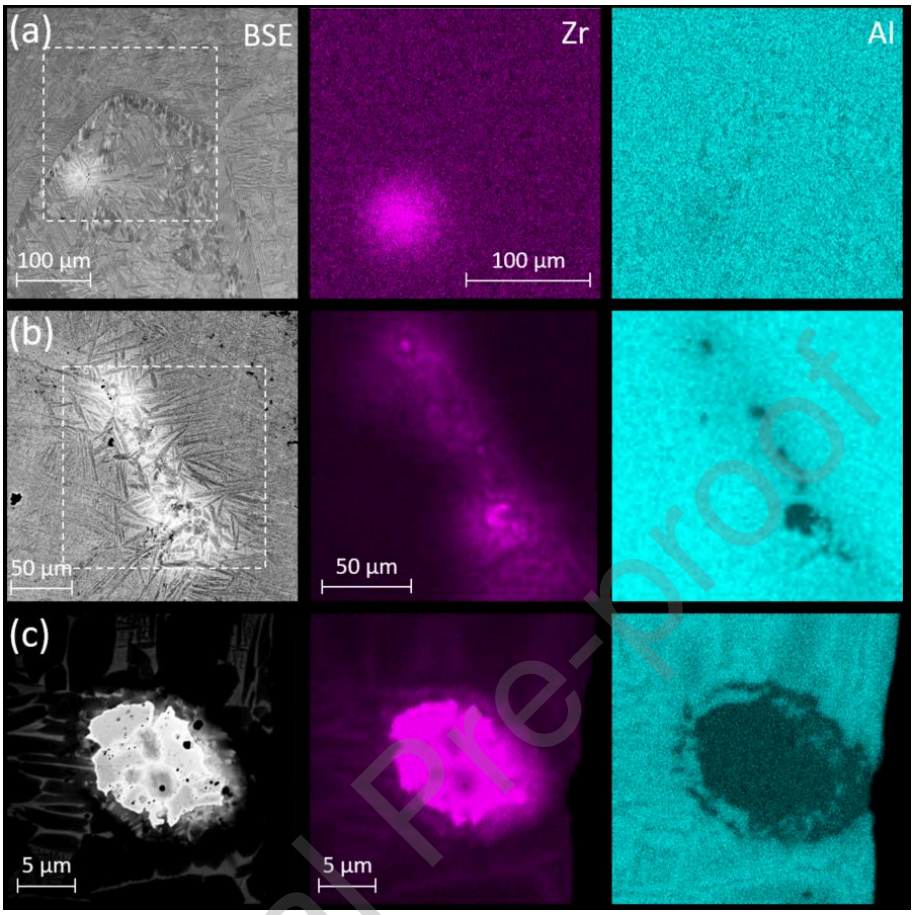

Figure 6: **BSE images and EDS maps of Zr rich regions; (a) near a prior β grain boundary, (b) a Zr rich solute band containing partially reacted ZrN particles and (c) a remaining polycrystalline ZrN particle near the sample edge.**

5.0 DISCUSSION

From the above results it is apparent that the TiN powder was very effective in grain refining the primary β phase under WAAM melt-pool conditions, whereas ZrN additions were not, even though some surviving ZrN particles were also found within the samples. In the current work the two nitride powders were added at relatively low addition levels (Table 2), which are representative of commercial practice with recognized grain refining systems [41]. In both cases the powders were found to be heterogeneously distributed, with the TiN particles appearing predominantly in clusters (Figure 4) and the partially dissolved ZrN particles being present in bands associated with an increased local Zr content (Figure 6). This indicates that both powders were not fully dispersed in the liquid phase, despite melt pool circulation being known to occur in the WAAM process due to the presence of arc forces and Marangoni convection [16]. This tendency for particle clustering may have been exacerbated by the use of the adhesive and its pyrolysis by the plasma torch before melting occurred. In comparison to the TiN powder, the larger ZrN particles appeared to have dispersed better in the melt and this may have been aided by their greater extent of dissolution. The large particle size difference between the powders is probably also important in this regard, with a stronger tendency for agglomeration seen for the finer TiN powder.

With the Ti64 alloy a low tendency for constitutional supercooling is expected at the solidification front in the WAAM process because little solute partitioning of V and Al occurs in Ti alloys [11] and there will be a relatively steep positive liquid thermal gradient (G_L) in a translated melt pool, due to the application of a high energy heat source with a cold substrate. The high effectiveness of TiN as a grain refiner under these adverse conditions is therefore encouraging. Trace elements in Ti64, such as Fe (K = 0.36 [42]), partition much more strongly than V and Al and may be important in this regard, but are present in low concentrations (<0.2 wt%.). The results in Figure 3a therefore suggest TiN particles must be highly efficient inoculants capable of stimulating nucleation ahead of the solidification front at very low undercoolings.

In the WAAM process the particles that entered the melt pool from the top surface, ahead of the torch as it moves forward, will circulate due to convection and interact with the solidification front at its rear and base. The solidification velocity (V) to liquid thermal gradient ratio (V/G_L) is an important factor contributing to the degree of constitutional supercooling. In a moving melt pool V/G_L varies considerably with position from the edge, where it is lowest and nucleation in the melt is less likely, to the centreline where it is highest [43]. The fact that there was a very abrupt change in grain structure when the TiN inoculant particles were added and that the refined grain size was nearly uniform across the build, in the sample shown in Figure 3, therefore, further suggests TiN is a very efficient nucleant.

Although some β grain growth is expected to have occurred during re-heating above the β transus as further layers are added, which would tend to reduce any local disparity in the grain size [20], little variation was seen in grain size with build height (Figure 3). In particular, the last added layer would not have been β annealed and shows a similar grain size to the rest of the refined part of build, which suggests that grain growth due to thermal cycling after solidification was not a significant effect in the samples studied.

5.1 Particle Stability

Research by Qiu et. al. [33] on nitride inoculation of Ti, using button melts with a β stabilised alloy (13%Mo-Ti), has suggested that with ZrN additions grain refinement occurs in a two stage process that first involves dissolution of Zr and N, followed by the precipitation of TiN into the melt, to form inoculating particles. They showed that when the ZrN particles fully dissolved, grain refinement was observed when the N content in the alloy must have exceeded at least ~ 0.4 wt %, which was inferred to indicate that this was the minimum N concentration required to precipitate TiN from the liquid in this alloy system. However, this concentration is a lot lower than the minimum level required to form TiN by a pro-peritectic reaction in the Ti-N binary system, which is at least ~ 5 wt% N [34]. Phase stability calculations completed with JmatPro 9.1 for the compositions of Ti64-TiN and Ti64-ZrN provided in Table 2 show, that with the order of magnitude lower addition levels used here, neither TiN nor ZrN are thermodynamically stable in the liquid phase. Ultimately, this means that when using low TiN and ZrN addition levels in Ti64 inoculation must occur directly from surviving particles, rather than by a dissolution and precipitation reaction, as previously reported with higher addtion levels in Ti-13Mo [33]. This means that the particles' dissolution kinetics relative to the melt contact time and temperature will be an important factor in determining their effectiveness. Care must then be taken when selecting particle sizes and addition levels as the distribution introduced to the melt will different from that which is present to participate in solidification precluding their usage from WAAM deposition strategies with higher heat inputs or long melt contact times, furthermore this may influence potential TiN/Ti64 feedstock manufacture. However, DED-AM is particularly well suited for inoculation by particles such as TiN which are not thermodynamically stable as

the particle/melt contact time is relatively short, furthermore, the lack of thermodynamic stability (especially for TiN) is a large positive for recyclability as any waste from WAAM can be included in conventional recycle streams without risking contamination by TiN particles.

Both TiN and ZrN have similar melting points of 2947 and 2952 ^{o}C, respectively [44], which are higher than that expected in the liquid Ti melt pool [39], so their decomposition in the melt pool will be primarily by dissolution rather than melting. Information on the dissolution kinetics of nitride particles in molten Ti are, however, difficult to obtain. TiN has been found to have a dissolution rate of ~2.2 µm/s in molten Ti-6242 at 1725^{o}C [45], which would mean that small particles should dissolve within melt contact times of a few seconds, but the dissolution behaviour is complex with both α stabilized and β interlayers observed to form between the TiN and liquid. In addition, liquid Ti has been found to readily infiltrate surface connected pores in TiN, which has been inferred to suggest that it readily wets nitride phases [45]. Melt pool fluid flow modelling has estimated the melt contact times to be of the order of four seconds with temperature exposures in the range of 1690 -2700 ^{o}C, for typical WAAM conditions, which suggests survival of larger particles, or clusters, should be possible [39].

5.2 Orientation relationships

Previous work on ZrN/TiN inoculation casting trials with a β stabilized Ti-13%Mo alloy by Qiu et al. [33], has directly measured two possible ORs by EBSD between TiN and β-Ti; the Nishiyama-Wassermann (NW), $\{111\}_{fcc}//\{1\bar{1}0\}_{bcc}$, $<\bar{1}01>_{fcc}//<001>_{bcc}$, or Kurdjumov-Sachs (KS), $\{111\}_{fcc}//\{1\bar{1}0\}_{bcc}$, $<\bar{1}10>_{fcc}//<\bar{1}11>_{bcc}$, with the NW preferred. These two orientation relationships (ORs) are classically expected between the BCC, β-Ti matrix, and FCC, NaCl-type crystal structure of TiN, and are closely related by a rotation angle of ~ 5°, which can make them difficult to distinguish. However, discrimination is within the capabilities of current EBSD systems, which have an angular resolution of ~ 1^{o} [46]. Adherence to one of these two ORs is strong evidence that grain refinement occurred by efficient heterogeneous nucleation of the primary β phase. This is because to occur at a low undercooling nucleation requires a low interface energy, which implies there must be at least partial coherency facilitated by a habit plane relationship between the inoculant particle and the new solid nucleus [47]. If the particles do not directly act as a heterogeneous nucleation sites, other mechanisms are possible that could aid nucleation, particularly within a particle cluster. For example, they could provide a locally solute enriched liquid environment with a different melting point. However, this first possibility does not apply to TiN, where N would disperse very rapidly, and Zr would reduce the local melting point within a particle cluster [48].

In order to evaluate the relative potential of TiN and ZrN to act as inoculants, their lattice matching can be compared to that of the solidifying high temperature β phase. The lattice parameters of the bcc β phase in Ti64 can be taken from the literature [49] (Table 4). When combined with its coefficient of thermal expansion (obtained from dilatometer tests), this allows extrapolation to the temperature range of interest. Similarly, published coefficients of thermal expansion and low temperature lattice parameters can be used to estimate the high temperature lattice parameters for the nitride phases (TiN [50] and ZrN [51] Table 4). The atomic mismatch obtained at melt pool temperature from these parameters for the two previously reported KS and NW, orientation relationships (ORs) are shown in Figure 7a, with schematic representations provided in Figure 7b. From this figure it can be seen that near the melting point of Ti64, the KS OR is more favourable for TiN compared to the NW OR, as the calculated mismatch (6%) is less than that for the NW OR. In comparison, ZrN exhibits a greater mismatch (>10%) than TiN with both ORs, as shown in Table 4. In addition, with ZrN the NW OR

misfit is higher than the expected limit for forming a semi-coherent interface. This means that while TiN may nucleate β Ti via the KS, or NW OR (with the KS OR preferred,) and ZrN may also nucleate via the KS OR, it is unlikely it will directly nucleate β Ti via the NW OR. However, since the lattice mismatch is less for TiN, the energy barrier for nucleation will be lower. In addition, there will be a smaller chemical contribution to the interface energy for TiN, as it will have Ti atoms occupying the interface plane, rather than Zr. This is reflected in the results obtained experimentally, where inoculation with TiN was found to be much more successful and resulted in substantial grain refinement of the WAAM build, whereas the ZrN particles achieved little observable grain refinement.

Table 4: Physical constants, estimated lattice parameters and predicted OR misfits at 1600 °C

Material	Lattice Parameters		Misfit (%)	
	a_o (Å)	a (Å) (1600 °C)	KS	NW
Ti64	3.31 (963°C) [49]	3.33	-	-
TiN	4.26 (25°C) [50]	4.33	6.0	11.4
ZrN	4.60 (-273°C) [51]	4.64	12.5	17.5

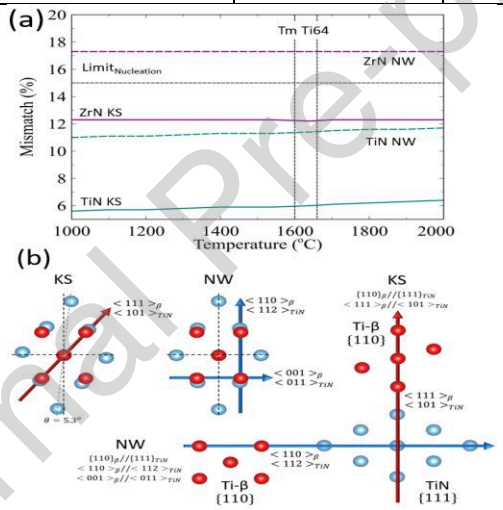

Figure 7: ZrN, TiN and Ti64 lattice orientation relations showing; (a) the lattice mismatch with the NW and KS OR as a function of temperature. In (b) schematics are provided of i) the KS and ii) NW ORs between TiN and Ti64.

5.3 TiN Inoculation

To investigate the mechanism of refinement further, more detailed characterization was performed of the clusters of TiN particles typified in Figure 4, using higher resolution EBSD accompanied by EDS. Two such examples are provided in Figure 8. The particles in the clusters were first identified as TiN by EDS, which showed a high local nitrogen content and absence of Al. This was then confirmed by successfully indexing EBSD patterns from the particles using the ideal NaCl crystal structure. Unfortunately, automated reconstruction of the matrix β grains from the orientations of the transformed α variants was not successful close to the cluster-matrix interface or for the small α grains found between the TiN particles in the clusters. This issue occurred because the reconstruction algorithm requires several neighbouring α variants to be indexed to correctly identify a parent β orientation, which was not possible within the cluster. The un-indexed and non-reconstructed regions have been left black in the EBSD maps in Figure

9. Poor β reconstruction close to the clusters, compounded by the use of 2D sectioning to characterize 3D particle clusters and the presence of multiple β grains growing from each cluster, also made it difficult to determine which TiN particle was responsible for nucleating each β grain.

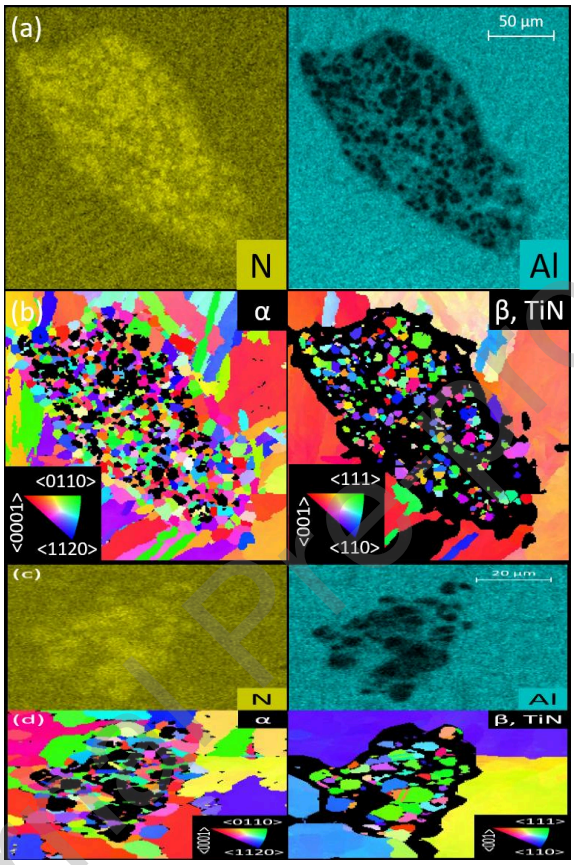

Figure 8: Higher magnification SEM-EBSD investigation of two typical TiN particle clusters: (a, c) EDS maps for C, N and Al for cluster 1 and 2, respectively, and (b, d). corresponding IPF||ND orientation maps for TiN, α-Ti and the reconstructed β-Ti grains.

As the matrix β grains could not be automatically reconstructed close to the interface of individual TiN particles, the room temperature, transformed, α orientations in the EBSD data were used to determine if there was statistical coincidence between the reported ORs for individual TiN particles within a cluster and the matrix. This was achieved by combining the BOR between α and β Ti with the NW, or KS, relationship between β Ti and TiN. Conveniently, the BOR has the same $\{110\}_\beta//\{0001\}_\alpha$ habit plane relationship as for the NW and KS ORs. As can be seen in the inset schematic in Figure 9a, for transformed α, the combined BOR + KS relationship can therefore be expressed in the same plane and direction of the β phase, as $\{111\}_{TiN}//\{0001\}_\alpha$ and $\langle 101\rangle_{TiN}//\langle 1\bar{1}20\rangle_\alpha$, while the NW OR is similar, but exhibits a 5° rotation. Using this method, the angular deviation from the BOR + KS ideal relationship can be directly reported using the orientation information obtained from OI Channel 5 software, in terms of a relative frequency distribution, as shown in Figure 9a. In this plot a deviation angle of close to 0° indicates a KS relationship, while a peak in the deviation angle at 5°, or 55°, would

suggest the NW OR is present. In Figure 10a it can be seen that the most highly preferred orientation between the particles in the clusters and the surrounding matrix grains has a deviation of < 2° from the KS orientation relationship. In comparison, the angular deviation distribution for the rest of the particles is more indicative of a typical random misorientation distribution [52]. The location of the boundaries that complied with the KS relation can also be identified and are shown in the maps in Figure 9 (b) and (c) (where interfaces with less than 1° deviation from the KS OR have been indicated by white lines). Interfaces which obeyed the KS OR were found both internally within the cluster, where some TiN particles were in contact with ingress of molten Ti (as shown inset in Figure 4a), and on particles that had external surfaces in contact with the surrounding β grains. Due to the 3D nature of the clusters, it was however difficult to retrospectively attribute a specific interface with the nucleation of a given matrix β grain. For example, either the external coincident interfaces, or interfaces within the clusters, could have formed first by heterogeneous nucleation of a thin β layer on a specific particle, which may then have grown outwards, or become trapped within the cluster, or cut off by other growing nuclei.

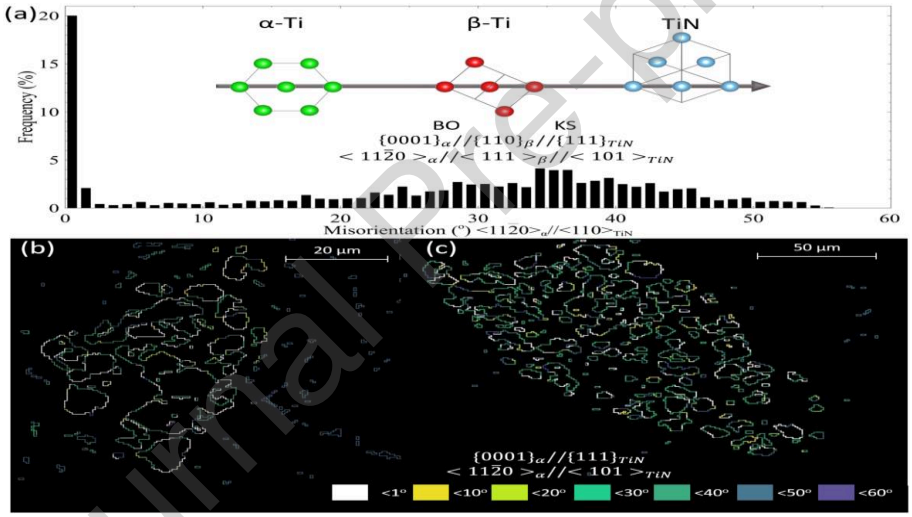

Figure 9: Determination of the statistical adherence of particles within TiN particle clusters to the KS OR with β matrix grains; (a) a misorientation distribution showing the relative frequency of the measured deviation from the KS between the TiN particles from the two TiN clusters in Figure 8, with the inset providing a schematic of the double orientation relationship between α and β to TiN. In (b) and (c) TiN/ α, KS OR boundary disorientation maps are shown for the particles in the two TiN clusters, where interfaces with less than 1° deviation from the KS OR have been indicated by white lines.

While the strong peak near 0° in the KS deviation angle frequency distribution in Figure 10 (a) demonstrates that this OR dominates, it does not completely preclude the possibility of some particles adopting the NW OR, as reported by Qiu et al. [33] in a different Ti-13%Mo alloy. This is because the difference of only 5^{o} misorientation between the NW and KS ORs could potentially lie within the error in the EBSD measurements when combined with the small misorientations in the BOR caused by the β to α transformation. Nevertheless, when taken together, the EBSD orientation data and theoretical lattice misfit calculations suggest a strong

preference for the KS OR. Furthermore, although it was not possible to reliably reconstruct the β grains close to the TiN particle clusters, multiple particles have been shown to have the KS orientation relationship with the several matrix β grains found to grow from each cluster, and it can therefore be concluded that they acted as heterogeneous nuclei with this preferred OR.

5.4 ZrN inoculation

Compared to the highly effective inoculation seen with TiN particle clusters, the ZrN powder did not have anywhere as significant an effect on the β grain size, nor the strength of the <001>//ND texture normally found in columnar WAAM grain structures. While many regions were found exhibiting local Zr enriched bands in the center of the Ti64-ZrN build (Figure 6) few surviving particles were observed large enough to be indexed by EBSD (shown in Figure 6c). More surviving ZrN particles were found located within grains near the surfaces of the build and their presence may have been responsible for the finer, non-<001>//ND fibre orientated, grains seen near the edges of this sample in Figure 2 (a). The example particle shown in Figure 10 came from such a near-surface region. In contrast to the TiN particles shown above (Figure 9), which exhibited multiple β grains growing from particle clusters, reconstruction of the far-field matrix β grain orientations for this particle showed it to be solely contained within a single β grain (Figure 11), which is more in agreement with expectation for inoculation by a single particle [18,50]. However, the particle shown in Figure 10 (a) was polycrystalline, containing several different orientations that corresponded to grains, rather than it being formed by a cluster of individual particles.

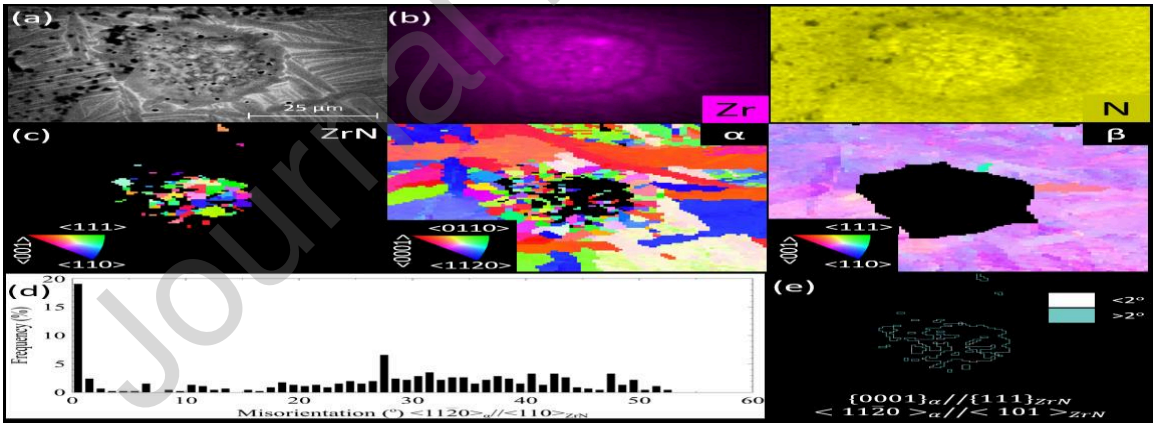

Figure 10: SEM investigation of ZrN particle (a) BSE image, (b) EDX Zr and N count map and IPF ND orientation maps for (c) ZrN, α-Ti and reconstructed β-Ti, along with misorientation between ZrN particles and α Ti at their interface (d) distribution plot, (e) misorientation map

Since the ZrN particles are polycrystalline, it was again difficult to identify which grain may have been responsible for nucleation of the surrounding matrix β grain. A similar analysis of the matrix-particle interface deviation from the KS OR was therefore conducted as for the TiN particle clusters. The corresponding resultant KS OR deviation angle relative frequency plot and interface map are shown in Figure 10 (d) and (e). The frequency plot again indicates that the KS OR relation was favoured between ZrN and β-Ti, but in the misorientation map there was not a

single contiguous interface, which obeyed the KS OR relationship, so it remained unclear if with this example particle the original nucleus for the surrounding matrix β grain formed in the cross section imaged.

The bulk chemical analysis showed that in the experiment here, in terms of volume, a similar amount of ZrN powder was introduced in to the melt as when the TiN powder was used (Table 3). However, the ZrN particles used were an order of magnitude larger than the TiN particles, so that there would have been 100 times fewer ZrN particles present in the melt pool than for the TiN, although this will have been counteracted by the strong tendency for the finer TiN particles to form large clusters of multiple particles which contained numerous particles (up to 100).

Overall, therefore, it is thus likely that, although the greater lattice mismatch makes it less efficient, nucleation is still possible directly from ZrN particles that remain undissolved within the melt pool in the WAAM process. Zr solute is also released as the particles dissolve, which has been claimed [36] to be beneficial by providing additional constitutional undercooling and growth restriction that will not be present in the case of TiN. These conditions appear to have been more prevalent near the edge of the deposit where there will have been shorter melt contact times, combined with a lower melt temperature, which led to a larger number of particles surviving in the melt pool.

6.0 CONCLUSIONS

The feasibility of exploiting TiN, or ZrN cubic nitride inoculants as grain refiners in high deposition rate Wire-Arc AM with titanium alloys like Ti64, has been successfully demonstrated at low addition levels. This approach has been previously investigated in casting, but not studied before for AM. In this investigation a relatively simple method was adopted for adding the particles to the melt pool, owing to the significant technical challenges of producing new Ti wires containing particulate grain refiners. Nevertheless, the results still enabled a successful comparison to be preformed of the efficacy of the two nitride compounds trialed.

- The TiN particles were found to be highly effective in refining the very coarse columnar β solidification structure normally seen in Ti64 builds produced by the WAAM process. A large reduction in grain size was observed, from the cm scale to an average of ~300 μm, as well as elimination of the highly-textured, columnar grain morphology, in favour of randomly orientated equiaxed grains. Due to the low undercooling conditions prevalent in AM melt pools with alloys like Ti64, it can thus be inferred that TiN is a very efficient β-Ti inoculant, even without the addition of solutal growth restricting elements.
- Due to the addition method employed, the fine TiN powder used was not effectively dispersed and formed clusters in the melt. However, individual particles within each cluster were found to match the Kurdjumov-Sachs orientation relationship with the β matrix, indicating successful inoculation. This was determined using a statistical methodology to correlate the orientation of the TiN particles with that of the matrix β grains, via the BOR, by mapping the orientations of the transformed α phase variants at the particles' interfaces.

- In comparison, the ZrN particles tested did not exhibit the same potent grain refinement observed with TiN. While some grain refining potential was demonstrated, the ZrN particles did not provide a sufficient density of nucleation events to induce a CET in the WAAM samples. This was shown to be caused partly by poorer lattice matching of ZrN with β Ti, but also due to the particles' lower survivability in the melt.
- It is also apparent from this study that a key technical challenge for implementing cubic nitride inoculation in AM is to develop an optimised method for introducing the particles that more evenly disperses them within the melt pool at low controlled dose rates.

ACKNOWLEDGEMENTS

The authors are appreciative of the EPSRC programme grant NEWAM (EP/R027218/1) and the Innovate UK project Open Architecture Additive Manufacturing (OAAM) for supporting aspects of this research. The authors acknowledge the use of equipment within Advanced Metals Processing and Characterisation themes of the Henry Royce Institute for Advanced Materials, funded through EPSRC grants EP/R00661X/1, EP/S019367/1, EP/P025021/1 and EP/P025498/1. P.B. Prangnell is also grateful to the Royal Academy of Engineering, UK, and Airbus for supporting his research through the Airbus-University of Manchester Centre for Metallurgical Excellence.

REFERENCES

[1] G. Lütjering, J.C. Williams, Titanium, Springer Science & Business Media, 2007.
[2] G. Welsch, R. Boyer, E.W. Collings, Materials Properties Handbook: Titanium Alloys, ASM International, 1993.
[3] W.J. Sames, F.A. List, S. Pannala, R.R. Dehoff, S.S. Babu, The metallurgy and processing science of metal additive manufacturing, Int. Mater. Rev. 61 (2016) 315–360. https://doi.org/10.1080/09506608.2015.1116649.
[4] A. Shokrani, I. Al-Samarrai, S.T. Newman, Hybrid cryogenic MQL for improving tool life in machining of Ti-6Al-4V titanium alloy, J. Manuf. Process. 43 (2019) 229–243. https://doi.org/10.1016/j.jmapro.2019.05.006.
[5] T. Duda, L.V. Raghavan, 3D Metal Printing Technology, IFAC-Pap. 49 (2016) 103–110. https://doi.org/10.1016/j.ifacol.2016.11.111.
[6] A.Y. Alfaify, J. Hughes, K. Ridgway, Critical evaluation of the pulsed selective laser melting process when fabricating Ti64 parts using a range of particle size distributions, Addit. Manuf. 19 (2018) 197–204. https://doi.org/10.1016/j.addma.2017.12.003.
[7] G. Nicoletto, R. Konečná, M. Frkáň, E. Riva, Surface roughness and directional fatigue behavior of as-built EBM and DMLS Ti6Al4V, Int. J. Fatigue. 116 (2018) 140–148. https://doi.org/10.1016/j.ijfatigue.2018.06.011.
[8] H. Zhao, A. Ho, A. Davis, A. Antonysamy, P. Prangnell, Automated image mapping and quantification of microstructure heterogeneity in additive manufactured Ti6Al4V, Mater. Charact. 147 (2019) 131–145. https://doi.org/10.1016/j.matchar.2018.10.027.
[9] S.W. Williams, F. Martina, A.C. Addison, J. Ding, G. Pardal, P. Colegrove, Wire + Arc Additive Manufacturing, Mater. Sci. Technol. 32 (2016) 641–647. https://doi.org/10.1179/1743284715Y.0000000073.
[10] F. Martina, J. Mehnen, S.W. Williams, P. Colegrove, F. Wang, Investigation of the benefits of plasma deposition for the additive layer manufacture of Ti–6Al–4V, J. Mater. Process. Technol. 212 (2012) 1377–1386. https://doi.org/10.1016/j.jmatprotec.2012.02.002.

[11] M.J. Bermingham, S.D. McDonald, M.S. Dargusch, D.H. StJohn, Grain-refinement mechanisms in titanium alloys, J. Mater. Res. 23 (2008) 97–104. https://doi.org/10.1557/JMR.2008.0002.
[12] Z. Zou, M. Simonelli, J. Katrib, G. Dimitrakis, R. Hague, Refinement of the grain structure of additive manufactured titanium alloys via epitaxial recrystallization enabled by rapid heat treatment, Scr. Mater. 180 (2020) 66–70. https://doi.org/10.1016/j.scriptamat.2020.01.027.
[13] M.J. Bermingham, D.H. StJohn, J. Krynen, S. Tedman-Jones, M.S. Dargusch, Promoting the columnar to equiaxed transition and grain refinement of titanium alloys during additive manufacturing, Acta Mater. 168 (2019) 261–274. https://doi.org/10.1016/j.actamat.2019.02.020.
[14] J. Donoghue, A.E. Davis, C.S. Daniel, A. Garner, F. Martina, J. Quinta da Fonseca, P.B. Prangnell, On the observation of annealing twins during simulating β-grain refinement in Ti–6Al–4V high deposition rate AM with in-process deformation, Acta Mater. 186 (2020) 229–241. https://doi.org/10.1016/j.actamat.2020.01.009.
[15] P.A. Colegrove, A.R. McAndrew, J. Ding, F. Martina, P. Kurzynski, S. Williams, System Architectures for Large Scale Wire + Arc Additive Manufacture, in: tokyo, japan, 2016: p. 5.
[16] W. Ou, T. Mukherjee, G.L. Knapp, Y. Wei, T. DebRoy, Fusion zone geometries, cooling rates and solidification parameters during wire arc additive manufacturing, Int. J. Heat Mass Transf. 127 (2018) 1084–1094. https://doi.org/10.1016/j.ijheatmasstransfer.2018.08.111.
[17] D. Lunt, A thesis submitted to The University of Manchester for the degree of Doctor of Philosophy in the Faculty of Engineering and Physical Sciences, (n.d.) 246.
[18] F. Martina, P.A. Colegrove, S.W. Williams, J. Meyer, Microstructure of Interpass Rolled Wire + Arc Additive Manufacturing Ti-6Al-4V Components, Metall. Mater. Trans. A. 46 (2015) 6103–6118. https://doi.org/10.1007/s11661-015-3172-1.
[19] J.R. Hönnige, P. Colegrove, S. Williams, Improvement of microstructure and mechanical properties in Wire + Arc Additively Manufactured Ti-6Al-4V with Machine Hammer Peening, Procedia Eng. 216 (2017) 8–17. https://doi.org/10.1016/j.proeng.2018.02.083.
[20] J.R. Hönnige, A.E. Davis, A. Ho, J.R. Kennedy, L. Neto, P. Prangnell, S. Williams, The Effectiveness of Grain Refinement by Machine Hammer Peening in High Deposition Rate Wire-Arc AM Ti-6Al-4V, Metall. Mater. Trans. A. (2020). https://doi.org/10.1007/s11661-020-05781-6.
[21] D. Gosslar, R. Günther, U. Hecht, C. Hartig, R. Bormann, Grain refinement of TiAl-based alloys: The role of TiB2 crystallography and growth, Acta Mater. 58 (2010) 6744–6751. https://doi.org/10.1016/j.actamat.2010.08.040.
[22] A.L. Greer, A.M. Bunn, A. Tronche, P.V. Evans, D.J. Bristow, Modelling of inoculation of metallic melts: application to grain refinement of aluminium by Al–Ti–B, Acta Mater. 48 (2000) 2823–2835. https://doi.org/10.1016/S1359-6454(00)00094-X.
[23] M.J. Bermingham, S.D. McDonald, D.H. StJohn, M.S. Dargusch, Beryllium as a grain refiner in titanium alloys, J. Alloys Compd. 481 (2009) L20–L23. https://doi.org/10.1016/j.jallcom.2009.03.016.
[24] S. Roy, S. Suwas, S. Tamirisakandala, D.B. Miracle, R. Srinivasan, Development of solidification microstructure in boron-modified alloy Ti–6Al–4V–0.1B, Acta Mater. 59 (2011) 5494–5510. https://doi.org/10.1016/j.actamat.2011.05.023.

[25] S. Mereddy, M.J. Bermingham, D.H. StJohn, M.S. Dargusch, Grain refinement of wire arc additively manufactured titanium by the addition of silicon, J. Alloys Compd. 695 (2017) 2097–2103. https://doi.org/10.1016/j.jallcom.2016.11.049.
[26] I. Maxwell, A. Hellawell, A simple model for grain refinement during solidification, Acta Metall. 23 (1975) 229–237. https://doi.org/10.1016/0001-6160(75)90188-1.
[27] J.H. Luan, Z.B. Jiao, G. Chen, C.T. Liu, Effects of boron additions and solutionizing treatments on microstructures and ductility of forged Ti–6Al–4V alloys, J. Alloys Compd. 624 (2015) 170–178. https://doi.org/10.1016/j.jallcom.2014.11.008.
[28] A.L. Greer, Grain Refinement of Alloys by Inoculation of Melts, Philos. Trans. Math. Phys. Eng. Sci. 361 (2003) 479–495.
[29] M.-X. Zhang, P.M. Kelly, M. Qian, J.A. Taylor, Crystallography of grain refinement in Mg–Al based alloys, Acta Mater. 53 (2005) 3261–3270. https://doi.org/10.1016/j.actamat.2005.03.030.
[30] J.R. Kennedy, D. Daloz, B. Rouat, E. Bouzy, J. Zollinger, Grain refinement of TiAl alloys by isomorphic self-inoculation, Intermetallics. 95 (2018) 89–93. https://doi.org/10.1016/j.intermet.2018.02.001.
[31] M.J. Bermingham, S.D. McDonald, M.S. Dargusch, Effect of trace lanthanum hexaboride and boron additions on microstructure, tensile properties and anisotropy of Ti-6Al-4V produced by additive manufacturing, Mater. Sci. Eng. A. 719 (2018) 1–11. https://doi.org/10.1016/j.msea.2018.02.012.
[32] S. Tamirisakandala, R.B. Bhat, J.S. Tiley, D.B. Miracle, Grain refinement of cast titanium alloys via trace boron addition, Scr. Mater. 53 (2005) 1421–1426. https://doi.org/10.1016/j.scriptamat.2005.08.020.
[33] D. Qiu, D. Zhang, M.A. Easton, D.H. St John, M.A. Gibson, Refining As-cast β-Ti Grains Through ZrN Inoculation, Metall. Mater. Trans. A. 49 (2018) 1444–1449. https://doi.org/10.1007/s11661-018-4531-5.
[34] H.A. Wriedt, J.L. Murray, Binary alloy phase diagrams. Vol. 3., ASM, 1986.
[35] N. Gey, M. Humbert, The calculation of a parent grain orientation from inherited variants for approximate (b.c.c.–h.c.p.) orientation relations, J. Appl. Crystallogr. 35 (2002) 401–405. https://doi.org/10.1107/S0021889802005824.
[36] P.S. Davies, B.P. Wynne, W.M. Rainforth, M.J. Thomas, P.L. Threadgill, Development of Microstructure and Crystallographic Texture during Stationary Shoulder Friction Stir Welding of Ti-6Al-4V, Metall. Mater. Trans. A. 42 (2011) 2278–2289. https://doi.org/10.1007/s11661-011-0606-2.
[37] P.S.W. Davies, An investigation of microstructure and texture evolution in the Near-α titanium alloy timetal 834., in: 2009.
[38] A. Ho, H. Zhao, J.W. Fellowes, F. Martina, A.E. Davis, P.B. Prangnell, On the origin of microstructural banding in Ti-6Al4V wire-arc based high deposition rate additive manufacturing, Acta Mater. 166 (2019) 306–323. https://doi.org/10.1016/j.actamat.2018.12.038.
[39] Numerical analysis of heat transfer and fluid flow in multilayer deposition of PAW-based wire and arc additive manufacturing - ScienceDirect, (n.d.). https://www-sciencedirect-com.manchester.idm.oclc.org/science/article/pii/S0017931017352201?via%3Dihub (accessed October 6, 2020).
[40] A.E. Davis, C.I. Breheny, J. Fellowes, U. Nwankpa, F. Martina, J. Ding, T. Machry, P.B. Prangnell, Mechanical performance and microstructural characterisation of titanium alloy-

alloy composites built by wire-arc additive manufacture, Mater. Sci. Eng. A. 765 (2019) 138289. https://doi.org/10.1016/j.msea.2019.138289.
[41] T.E. Quested, A.L. Greer, The effect of the size distribution of inoculant particles on as-cast grain size in aluminium alloys, Acta Mater. 52 (2004) 3859–3868. https://doi.org/10.1016/j.actamat.2004.04.035.
[42] X. Liu, G. Feng, Y. Zhou, Q. Fan, Macrosegregation and the underlying mechanism in Ti-6.5Al-1.0Cr-0.5Fe-6.0Mo-3.0Sn-4.0Zr alloy, Prog. Nat. Sci. Mater. Int. 29 (2019) 224–230. https://doi.org/10.1016/j.pnsc.2019.02.006.
[43] Welding: Solidification and microstructure | SpringerLink, (n.d.). https://link-springer-com.manchester.idm.oclc.org/article/10.1007/s11837-003-0134-7 (accessed October 6, 2020).
[44] "Physical Constants of Organic Compounds," in CRC Handbook of Chemistry and Physics, 101st Edition (Internet Version 2020), John R. Rumble, ed., CRC Press/Taylor & Francis, Boca Raton, FL (accessed October 7, 2020).
[45] B.P. Bewlay, M.F.X. Gigliotti, Dissolution rate measurements of TiN in Ti-6242, Acta Mater. 45 (1997) 357–370. https://doi.org/10.1016/S1359-6454(96)00098-5.
[46] F.J. Humphreys, Review Grain and subgrain characterisation by electron backscatter diffraction, J. Mater. Sci. 36 (2001) 3833–3854. https://doi.org/10.1023/A:1017973432592.
[47] M.-X. Zhang, P.M. Kelly, Edge-to-edge matching model for predicting orientation relationships and habit planes—the improvements, Scr. Mater. 52 (2005) 963–968. https://doi.org/10.1016/j.scriptamat.2005.01.040.
[48] M.A. Turchanin, P.G. Agraval, A.R. Abdulov, Thermodynamic assessment of the Cu-Ti-Zr system. II. Cu-Zr and Ti-Zr systems, Powder Metall. Met. Ceram. 47 (2008) 428. https://doi.org/10.1007/s11106-008-9039-x.
[49] J.W. Elmer, T.A. Palmer, S.S. Babu, E.D. Specht, In situ observations of lattice expansion and transformation rates of α and β phases in Ti–6Al–4V, Mater. Sci. Eng. A. 391 (2005) 104–113. https://doi.org/10.1016/j.msea.2004.08.084.
[50] E. Mohammadpour, M. Altarawneh, J. Al-Nu'airat, Z.-T. Jiang, N. Mondinos, B.Z. Dlugogorski, Thermo-mechanical properties of cubic titanium nitride, Mol. Simul. 44 (2018) 415–423. https://doi.org/10.1080/08927022.2017.1393810.
[51] J. Kim, Y.J. Suh, Temperature- and pressure-dependent elastic properties, thermal expansion ratios, and minimum thermal conductivities of ZrC, ZrN, and Zr(C0.5N0.5), Ceram. Int. 43 (2017) 12968–12974. https://doi.org/10.1016/j.ceramint.2017.06.195.
[52] J.K. Mason, C.A. Schuh, The generalized Mackenzie distribution: Disorientation angle distributions for arbitrary textures, Acta Mater. 57 (2009) 4186–4197. https://doi.org/10.1016/j.actamat.2009.05.016.

Declaration of interests

☒ The authors declare that they have no known competing financial interests or personal relationships that could have appeared to influence the work reported in this paper.

☐The authors declare the following financial interests/personal relationships which may be considered as potential competing interests:

2021-02-23

The potential for grain refinement of wire-arc additive manufactured (WAAM) Ti-6Al-4V by ZrN and TiN inoculation

Kennedy, Jacob R.

Elsevier

Kennedy JR, Davis AE, Caballero AE, et al., (2021) The potential for grain refinement of wire-arc additive manufactured (WAAM) Ti-6Al-4V by ZrN and TiN inoculation. Additive Manufacturing, Volume 40, April 2021, Article number 101928

https://doi.org/10.1016/j.addma.2021.101928